Neuron
Report

NMDA Receptor-Dependent Multidendrite Ca^{2+} Spikes Required for Hippocampal Burst Firing In Vivo

Christine Grienberger,[1] Xiaowei Chen,[1,2] and Arthur Konnerth[1,*]
[1]Institute of Neuroscience, Center for Integrated Protein Science and SyNergy Cluster, Technical University Munich, Biedersteiner Straße 29, Munich 80802, Germany
[2]Brain Research Center, Third Military Medical University, Chongqing 400038, China
*Correspondence: arthur.konnerth@lrz.tum.de
http://dx.doi.org/10.1016/j.neuron.2014.01.014

SUMMARY

High-frequency bursts of action potentials (APs) are a distinctive form of signaling in various types of mammalian central neurons. In CA1 hippocampal pyramidal neurons in vivo, such complex spike bursts (CSs) are detected during various behaviors and are considered to be particularly important for learning- and memory-related synaptic plasticity. Here, we combined whole-cell recordings and two-photon imaging in mouse CA1 pyramidal neurons to investigate the cellular mechanisms underlying CSs in vivo. Our results demonstrate that CSs are of synaptic origin, as they require N-methyl-D-aspartate (NMDA) receptor activation. We identify voltage-gated Ca^{2+} channel-dependent, spike-like depolarizations as integral components of the CSs. These Ca^{2+} spikes were invariably associated with widespread large-amplitude Ca^{2+} transients in basal and apical dendrites. Together, our results reveal a type of NMDA receptor-dependent multidendrite Ca^{2+} spike required for high-frequency bursting in vivo.

INTRODUCTION

High-frequency bursts of action potentials (APs) make an important contribution to information processing in central mammalian neurons (Harris et al., 2002). Such bursts were detected in hippocampal neurons of various species, including cats (Kandel and Spencer, 1961), rabbits (Fujita, 1975), rats (Buzsáki et al., 1996; Epsztein et al., 2011), and mice (Harvey et al., 2009), and may represent a general feature of neuronal signaling in the mammalian brain. While single APs can fail to reach connected downstream neurons, bursts are often transmitted more reliably (Izhikevich et al., 2003; Lisman, 1997). Thus, they can accelerate transmission of information (Kepecs et al., 2002). Remarkably, bursts are highly effective in the induction of synaptic plasticity (Paulsen and Sejnowski, 2000) and in the formation of hippocampus-dependent memories (Xu et al., 2012). Experimental evidence, obtained mostly in rats, indicates that under in vivo conditions, bursts in the hippocampus occur with a high incidence during specific behaviors, such as goal identification and approach (Ranck, 1973) or sleep and resting conditions (Suzuki and Smith, 1985). In the hippocampus, prolonged bursts of APs, referred to also as complex spike bursts (CSs), are detected during nontheta states as conditional synchrony detectors, mostly present after a period of neuronal silence (Harris et al., 2001). Two more recent studies demonstrated, using whole-cell recordings in head-fixed mice on a spherical treadmill or in freely moving rats exploring a maze, that hippocampal place cells exhibit spatially tuned CSs (Epsztein et al., 2011; Harvey et al., 2009).

The cellular mechanisms underlying bursting in hippocampal CA1 pyramidal neurons were studied previously almost exclusively in in vitro rat brain slices. A major focus of this research was the study of intrinsic mechanisms underlying the burst-generating spike afterdepolarization (e.g., Azouz et al., 1996; Metz et al., 2005). This work showed that the afterdepolarization involves K^+ channels (Jensen et al., 1994), Na^+ channels (Azouz et al., 1996), and Ca^{2+} channels (Metz et al., 2005). In line with these observations, the contribution of Ca^{2+} currents is augmented when K^+ channels are concomitantly blocked by pharmacological means (Magee and Carruth, 1999; Sanabria et al., 2001). The propensity for intrinsic bursting can vary between different CA1 pyramidal neurons. Thus, in addition to reliable bursters, there is also a subpopulation of "regular" spiking neurons (Jarsky et al., 2008; Jensen et al., 1994) and there is evidence that regular spiking and bursting CA1 neurons have distinct morphological features (Graves et al., 2012). Furthermore, theta-like repeated coincident stimulation of Schaffer collaterals (from the CA3 region) and the perforant path (from the entorhinal cortex) can produce plateau potentials in disinhibited hippocampal slices (Takahashi and Magee, 2009). These plateau potentials, which are initiated in the apical trunk and tuft region, can produce dendritically initiated APs. At present, it is unclear how plateau potential-mediated bursting relates to the CSs observed in vivo, as these are clearly detectable during nontheta states (Harris et al., 2001). This may indicate that additional or perhaps different synaptic mechanisms can drive spontaneous bursting in the intact hippocampus.

Here, we devised an approach to investigate the cellular mechanisms underlying CSs in mouse CA1 pyramidal neurons in vivo. For this purpose, we combined whole-cell recordings and two-photon dendritic Ca^{2+} imaging with various intra- and extracellular pharmacological manipulations. Our results demonstrate that CS firing in vivo is a feature that is in principle shared by all CA1 pyramidal neurons and that it requires

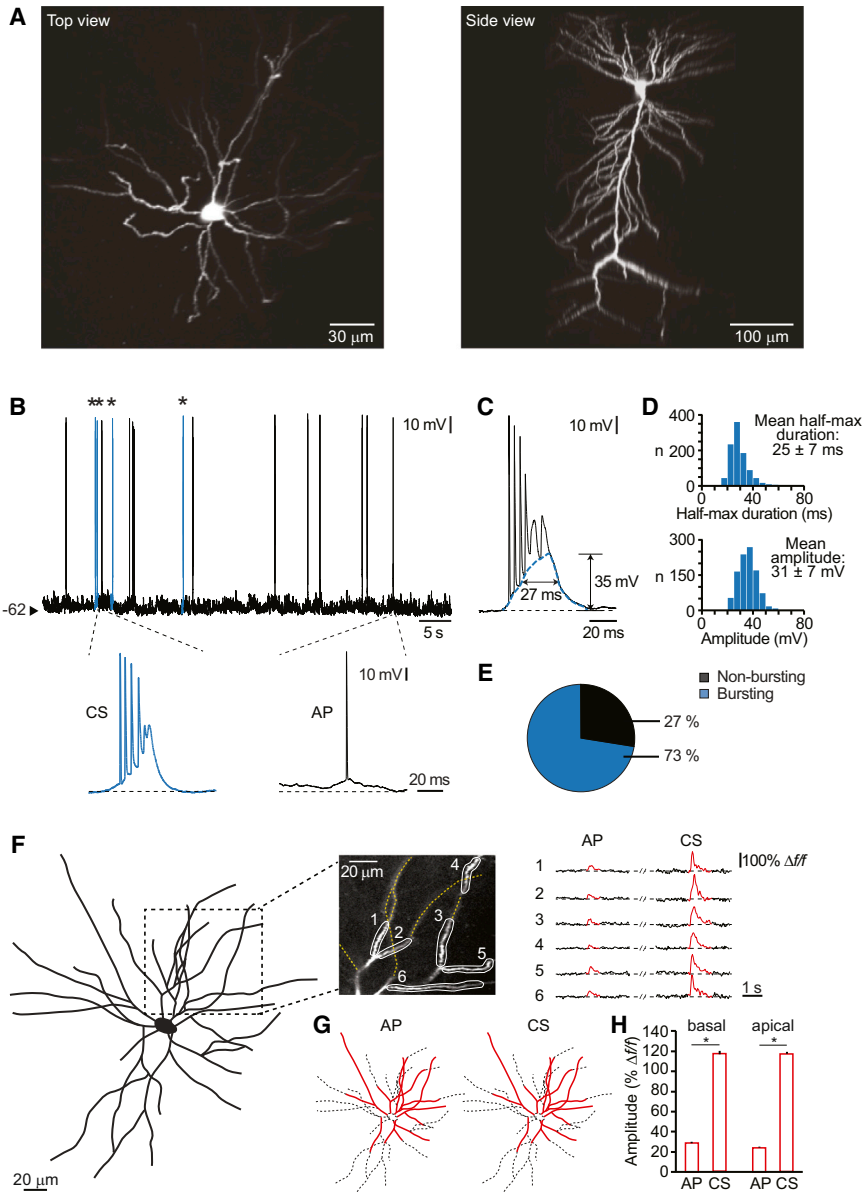

Figure 1. Complex Spike Bursts in a Fraction of In Vivo Visually Identified CA1 Pyramidal Neurons

(A) Three-dimensional reconstruction of a CA1 pyramidal neuron, labeled in vivo with Alexa Fluor 594. (B) Spontaneous activity, recorded in vivo from a CA1 pyramidal neuron. Complex spike bursts (CSs) are marked in blue and by asterisks (*). (C) Enlarged view of a CS. It consists of a depolarizing wave and a high-frequency train of action potentials (APs). (D) Histograms showing the distribution of the half-max durations (top) and amplitudes (bottom) of the depolarizing waves (n = 993 CSs from 30 neurons). (E) Pie chart of the proportion of bursting and nonbursting neurons (n = 30 neurons total). (F) Reconstruction from fluorescence images of basal dendrites of a CA1 pyramidal neuron (top view, leftmost panel). The dotted rectangle indicates the focal plane used for the imaging of dendritic Ca^{2+} signals associated with single APs and CSs (rightmost panel). The Ca^{2+} signals were recorded in regions of interest indicated in the fluorescence image (middle). (G) Summary of AP- and CS-associated dendritic Ca^{2+} activity (indicated in red) in regions imaged sequentially in five focal planes in the neuron shown in (F). Dotted lines indicate nonimaged dendrites. (H) Bar graph of amplitudes (mean ± SEM, in % $\Delta f/f$) of dendritic Ca^{2+} signals associated with single APs and CSs (basal: n = 105 basal dendritic segments from 12 neurons, Kolmogorov-Smirnov test, *$p < 0.001$; apical: n = 45 apical dendritic segments from 3 neurons, Kolmogorov-Smirnov test, *$p < 0.001$).

N-methyl-D-aspartate (NMDA) receptor-dependent synaptic transmission. We provide evidence that CSs require the activation of voltage-gated Ca^{2+} channels. The dendritic two-photon imaging experiments demonstrate large and widespread Ca^{2+} transients throughout basal and apical dendrites. Thus, our results identify NMDA receptor-dependent dendritic Ca^{2+} spikes as essential determinants for CS generation in CA1 pyramidal neurons in vivo.

RESULTS

Dendritic Ca^{2+} Imaging in Visually Identified CA1 Pyramidal Neurons In Vivo

Targeted in vivo whole-cell recordings of mouse hippocampal CA1 pyramidal neurons were obtained by applying the "shadow patching" approach (Kitamura et al., 2008). Direct visualization of the hippocampal neurons by means of two-photon imaging (Figure 1A; see Experimental Procedures) required the removal of a small portion (1–1.5 mm diameter) of the cortical tissue covering the hippocampus (Busche et al., 2012; Dombeck et al., 2010; Mizrahi et al., 2004). Figure 1B shows that under these conditions the electrical activity consisted of standard APs and characteristically shaped bursts of APs, which we refer to as CSs (Buzsáki et al., 1996). This pattern was similar to what has been found in the intact brain (Buzsáki et al., 1996; Epsztein et al., 2011; Harvey et al., 2009). Our results are not surprising in view of recent work (Dombeck et al., 2010) that reported unaltered hippocampal dynamics and place cell properties in awake mice with even larger cortical windows (2.7–2.8 mm diameter). Furthermore, the overall firing rate was 0.6 ± 0.11 Hz (mean ± SEM, n = 29 neurons) and, thus, similar to what has been found in intact brains of anesthetized mice (Hahn et al., 2007). Similarly, the fraction of bursts (Figure S1A available online) was comparable to that observed in rats during slow-wave sleep (Mizuseki and Buzsáki, 2013). Under our experimental conditions, CSs consisted of high-frequency trains (100–250 Hz) of mostly four to five APs of

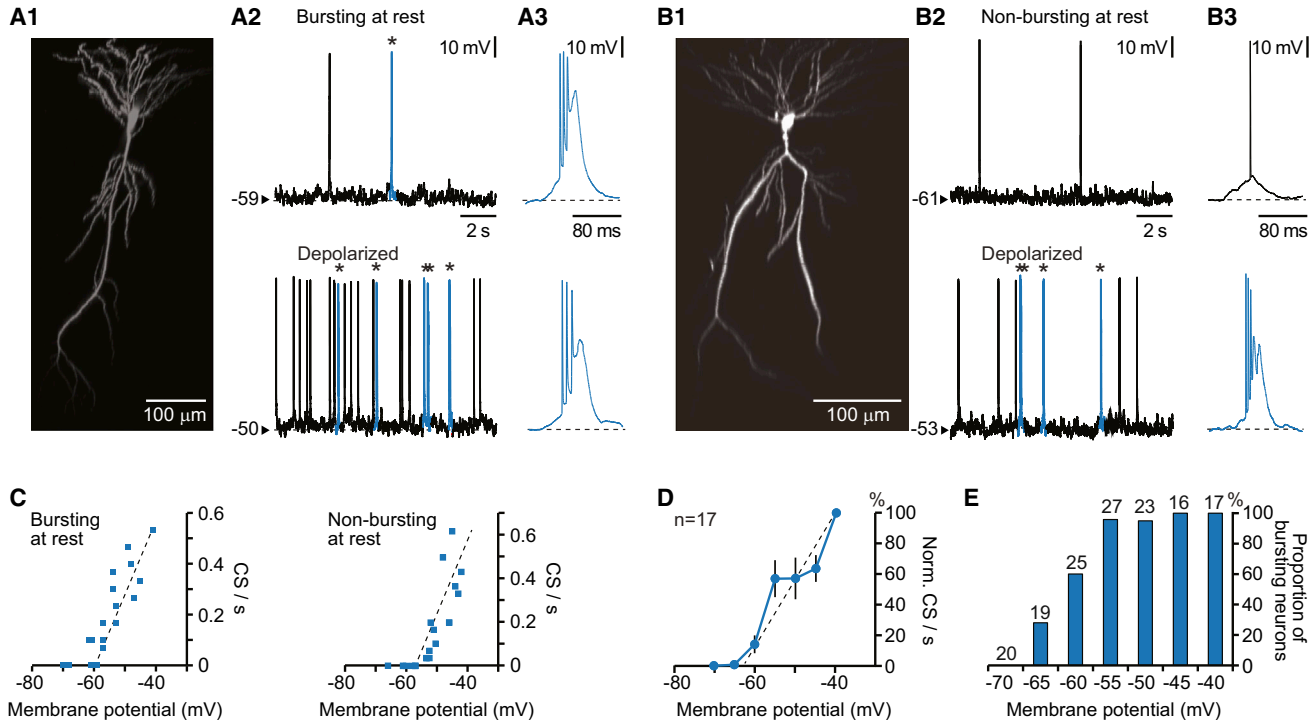

Figure 2. Dependence of Complex Spike Burst Frequencies on the Membrane Potential

(A1–B3) Spontaneous activity at two different membrane potentials, taken from two neurons that either fire CSs at resting membrane potential (A1–A3) or that do not fire CSs at resting membrane potential (B1–B3). CSs are marked in blue and by asterisks (*). (C) CS frequency. Data points are from the neurons shown in (A1)–(B3). (D) Normalized CS frequency (mean ± SEM, in %). (E) Proportion of bursting neurons. Note that since the number of experiments (n) contributing to each data point varied the actual n values are indicated by the small numbers next to the bars.

decreasing amplitude that were riding on a large depolarizing envelope or "wave." Figure 1C illustrates such a CS, in which the depolarizing wave (blue trace) had an amplitude of 35 mV and lasted at half-maximal amplitude for 27 ms. On average (n = 993 CSs from 30 neurons), the half-max duration of the depolarizing waves was 25 ± 7 ms and the amplitude was 31 ± 7 mV (mean ± SD) (Figure 1D). At resting potential (zero current through the patch pipette), CSs were observed in 73% of all the recorded neurons (Figure 1E). Overall, we conclude that our preparation is well suited for a detailed analysis of CSs, including two-photon Ca^{2+} imaging in combination with whole-cell recordings. Figures 1F–1H illustrate an example of such recordings, demonstrating that both single APs and CSs produced Ca^{2+} transients that invaded virtually all branches within the dendritic field. However, the CS-associated dendritic Ca^{2+} signals in the basal and proximal apical dendrites were clearly larger than those encountered with single APs (Figures 1G and 1H) as well as AP number-matched trains with similar AP frequency (Figure S1B).

Voltage Dependence of Complex Spike Bursts In Vivo

A distinct feature of CSs, which was not anticipated by previous in vitro work but consistent with earlier extracellular in vivo recordings (Harris et al., 2001), was the observation that their frequency increased strongly with depolarization. In the example illustrated in Figures 2A1–2A3, the depolarization of the baseline voltage from −59 mV to −50 mV caused a more than 4-fold increase in CS frequency (Figure 2C). Interestingly, apparent nonbursters, which are neurons that did not fire CSs at resting potential, started to burst as soon as these neurons were depolarized above −58/−60 mV by current injection through the patch pipette (Figures 2B1–2B3). Above this "bursting threshold," both bursters and nonbursters exhibited a similarly steep dependence of the CS frequency on the membrane voltage (Figures 2C and 2D; Figure S2A). This voltage dependence was observed in 31/31 tested neurons (Figure 2E, n = 8 were nonbursters at rest). Similarly, in all neurons tested (n = 7), brief depolarizing current injections (50 ms, 150 pA) could induce CSs with a probability of approximately 50% (Figure S2C). Together, these experiments demonstrate that CSs can be evoked in all CA1 hippocampal neurons in vivo and that voltage-dependent processes contribute, at least partially, to CS generation.

Synaptic Origin of Complex Spike Bursts

Spontaneous firing of CA1 pyramidal neurons in vivo, including CSs, is completely blocked by the combined application of the α-amino-3-hydroxy-5-methyl-4-isoxazolepropionic acid (AMPA) receptor antagonist CNQX and the NMDA receptor antagonist APV (Busche et al., 2012). Figures 3A–3D show that the intracellular application of MK-801, a use-dependent antagonist of NMDA receptors that works also from the inside, blocked

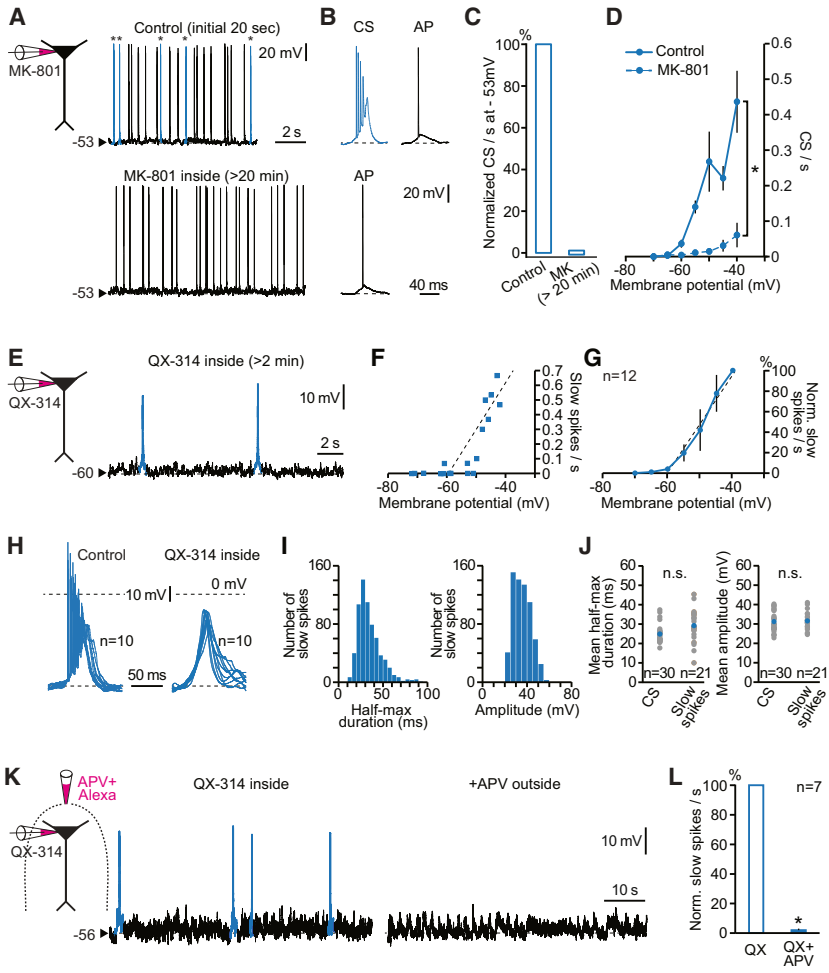

Figure 3. Synaptic Origin of Complex Spike Bursts

(A and B) Spontaneous activity during intracellular MK-801 application at −53 mV. Thirteen second period (A) and enlarged view (B) are shown. (C) Normalized CS frequency (mean ± SEM, in %) under MK-801. Data are from the experiment shown in (A). (D) Absolute CS frequency in control neurons and under MK-801 (n = 31 and 18 neurons, respectively, Kolmogorov-Smirnov test, −60 mV; *p < 0.01, −55 mV; *p < 0.001, −50 mV; *p < 0.001, −45 mV; *p < 0.001, −40 mV; *p < 0.001). (E) Spontaneous activity, recorded from a neuron under QX-314. Slow spikes are highlighted in blue. (F) Slow spike frequency. Data points are from the neuron shown in (E). (G) Normalized slow spike frequency (mean ± SEM, in %). (H) Overlay of ten CSs (left) and ten slow spikes (right). (I) Histograms showing the distribution of the half-max durations (left) and amplitudes (right) of the slow spikes (n = 664 from 21 neurons). (J) Comparison of the half-max durations (left) and amplitudes (right) of CSs and slow spikes. Shown are data points from individual animals (gray) and the mean values ± SEM in color; (half-max duration: 25 ± 1 ms and 30 ± 2 ms, Mann-Whitney test, p = 0.052; amplitude: 31 ± 1 mV and 31 ± 1 mV, Mann-Whitney test, p = 632). (K) Slow spikes are blocked by APV. (L) Normalized slow spike frequency (mean ± SEM, in %) before and during extracellular APV application (n = 7 neurons, Kolmogorov-Smirnov test, *p < 0.005).

CSs while AP firing persisted at a lower frequency (see also Figure S2C). This result demonstrates the synaptic origin of CSs and the critical role of NMDA receptors in their generation. In order to characterize the synaptic depolarization underlying CS firing, we blocked APs intracellularly by using QX-314 (Kamondi et al., 1998b; Strichartz, 1973). In these conditions, we observed slow spike-like potentials (Figures 3E–3J). These slow spikes were in many ways similar to the CS-associated depolarizing waves (Figure 3H). Thus, the slow spike frequency was similarly dependent on the membrane potential (Figures 3F and 3G; Figure S2B), the time courses and amplitudes were similar (Figures 3I and 3J), and, as in the case of CSs (Figure 2E), they were a common feature of all neurons (18/18; Figure S3A1). As expected, the NMDA antagonists APV (Figures 3K and 3L) and MK-801 (Figure S3A2) effectively suppressed the slow spikes. To exclude that the slow spikes were just an artifact produced by the intracellular use of QX-314, we inactivated APs by a sustained increase of the baseline membrane potential to about −35 mV. In these conditions, in the absence of any pharmacological treatment, we also recorded slow spikes that were similar to the CS-associated depolarizing waves (Figure S3B). Together, these results identify the slow spikes as critical determinants of CS firing in vivo.

Cellular Mechanisms Underlying Slow Spikes

Next, we used two-photon imaging to study the dendritic Ca^{2+} signals associated with the slow spikes. As CSs, slow spikes were associated with large Ca^{2+} transients in basal (Figures 4A1–4A3) and proximal apical dendrites (Figures S4A and S4C), as well as in the somata (Figures S4B and S4D). In addition, we identified smaller-amplitude Ca^{2+} transients in highly confined dendritic hot spots (Figures 4A1–4A3 and S4A), representing presumably asynchronous synaptic input sites (Jia et al., 2010). Importantly, the slow spike-associated large dendritic, but not the hot spot, Ca^{2+} transients were abolished by D-890 (Figures 4B1–4B3), an intracellular broad-range antagonist of voltage-gated Ca^{2+} channels in hippocampal (Conti and Lisman, 2002; Kovalchuk et al., 2000) and cortical neurons (Schiller et al., 2000). In parallel to the large dendritic Ca^{2+} transients, the slow spikes were also abolished by D-890 (Figures 4C–4E). Due to the limited access of functional two-photon Ca^{2+} imaging, we were not able to determine whether the asynchronous hot spot Ca^{2+} signals represented local dendritic spikes (Schiller et al., 2000) or single spine responses (Chen et al., 2011). In line with the NMDA receptor sensitivity of the CSs (Figures 3A–3D; Figure S2C) and of that of synaptic input sites (Jia et al., 2010), we found that APV blocked effectively both the large dendritic as well as the hot spot Ca^{2+} transients (Figures 4F and 4G). The large dendritic Ca^{2+} transients were never observed in isolation in single dendritic branches. Instead, they were reliably detected in all branches within the field of view

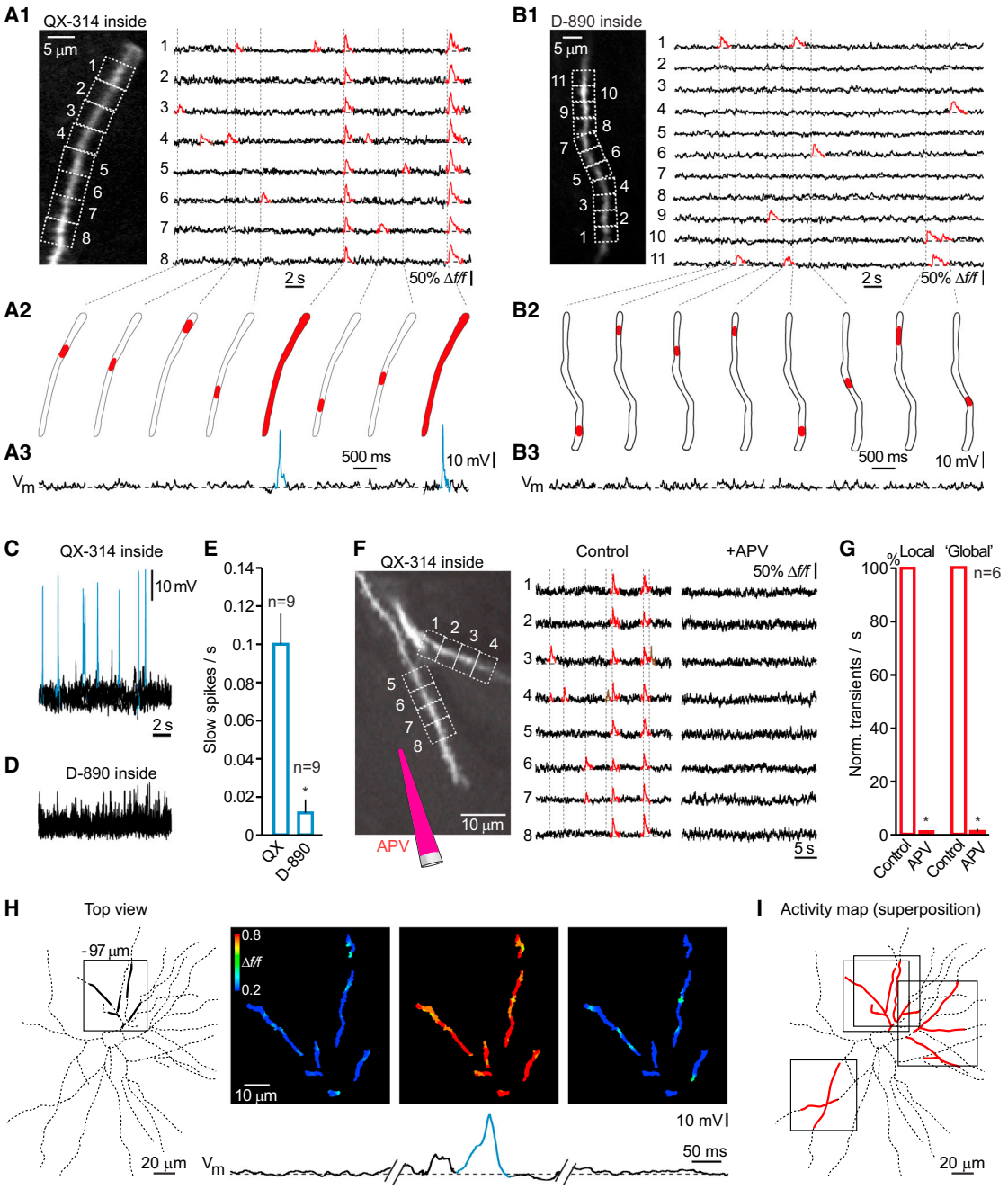

Figure 4. Slow Spikes Are NMDA Receptor Dependent Multidendrite Ca^{2+} Spikes

(A1) Left: two-photon image of a dendritic branch in the presence of QX-314 inside. Right: spontaneous Ca^{2+} transients in the ROIs 1–8 (3 × 4 µm size). (A2 and A3) Corresponding Ca^{2+} signals (red, A2) and membrane potential (A3, slow spike in blue). (B1) Left: two-photon image of a dendritic branch (with D-890 inside). Right: spontaneous Ca^{2+} transients in the ROIs 1–11 (3 × 4 µm size). (B2 and B3) Corresponding Ca^{2+} signals (red, B2) and membrane potential (B3). Dotted lines indicate corresponding events. (C) Overlay of ten consecutive membrane potential recordings (15 s each) (with QX-314 inside). (D) Overlay of ten consecutive membrane potential recordings (15 s each) (with D-890 inside). (E) Slow spike frequencies (mean ± SEM) in the presence of QX-314 and D-890 (Kolmogorov-Smirnov test, *$p < 0.05$). Membrane potential was −55 mV. (F) Left: two-photon image of a neuron and scheme of drug-application pipette containing APV and Alexa 594. Dashed boxes indicate the ROIs for Ca^{2+} signal monitoring. Right: Ca^{2+} recordings before (control) and during APV application. Fluorescence images in (A), (B), and (F) are averages of 1,200 frames. (G) APV block of local and "global" Ca^{2+} transients (summary of n = 6 cells) (mean ± SEM, Kolmogorov-Smirnov test, *$p < 0.001$). (H) Reconstruction of basal dendrite morphology of a CA1 pyramidal neuron (top view, leftmost panel). Dotted lines represent the out-of-focus dendrites. The rectangle indicates the focal plane used for the imaging of Ca^{2+} signals that are shown in pseudocolor images (right panels) before, during, and after a slow spike (blue trace bottom). (I) Dendritic Ca^{2+} signals (red) associated slow spikes. Activity map was obtained by the superposition of four focal planes (rectangles) that were imaged sequentially.

(Figures 4H and 4I) and corresponded strictly with all slow spikes, without failures in all 14/14 neurons tested.

DISCUSSION

Our results provide critical mechanistic insights into the generation of CSs in CA1 pyramidal neurons in vivo. By combining targeted whole-cell recordings, two-photon imaging of dendritic Ca^{2+} signals, and pharmacological manipulations in vivo, we show that CSs can occur in all CA1 pyramidal neurons, provided that they are sufficiently depolarized. CSs are induced by synaptic excitation and require the combined activation of NMDA receptors and voltage-gated Ca^{2+} channels, which together produce a nonlinear regenerative spike-like response engaging basal and apical dendrites. While previous in vitro work has focused on the role of intrinsic membrane properties for burst firing (Azouz et al., 1996; Jensen et al., 1994; Metz et al., 2005), we now establish that in vivo CSs have in addition a pronounced synaptic component (see also Abraham and Kairiss, 1988; Rose et al., 1984). This may explain why CSs in vivo consist typically of five, and sometimes even more, APs rather than the usual two APs detected in the subset of bursting CA1 pyramidal neurons in vitro.

Dendritic Ca^{2+} Imaging in CA1 Pyramidal Neurons In Vivo

Since these are the first dendritic Ca^{2+} recordings in CA1 pyramidal neurons in vivo, we would like to mention several technical considerations that are relevant for such experiments. First, the surgical removal of a small portion of cortical tissue is a possible point of concern for the study of cognitive processes. However, on the cellular level, the basic patterns of hippocampal activity are highly similar in intact brains (Harvey et al., 2009; Mizuseki and Buzsáki, 2013; Mizuseki et al., 2011) and in those with cortical windows (Busche et al., 2012; Kandel and Spencer, 1961; Kuga et al., 2011; Mizrahi et al., 2004). For example, there is a close similarity of CS frequencies in both preparations (Hahn et al., 2007). Furthermore, even theta oscillations and place cell activity, requiring an intact hippocampal circuitry, were not affected by such cortical windows (Dombeck et al., 2010). Second, the mechanical stabilization of the hippocampal tissue with agarose was an essential factor for good dendritic Ca^{2+} recordings in hippocampal neurons. Third, as for dendritic recordings in cortical neurons (Chen et al., 2011; Jia et al., 2010; Varga et al., 2011), dendritic Ca^{2+} imaging in the hippocampus in vivo required long-term (>40 min) high-quality whole-cell recordings with a sufficiently low access resistance (<50 MOhm).

A New Type of NMDA Receptor-Dependent Multidendrite Ca^{2+} Spike in Hippocampal Neurons

It has been known for many years that CA1 pyramidal neurons in brain slice preparations can produce, under certain pharmacological conditions (e.g., the presence of TTX), Ca^{2+} spikes. These had smaller amplitudes but longer durations than regular APs (Benardo et al., 1982; Golding et al., 1999; Schwartzkroin and Slawsky, 1977; Wong et al., 1979). Since these Ca^{2+} spikes were typically evoked experimentally by injections of strong and long-lasting depolarizing currents, it remained unclear whether they occur also in the intact hippocampus in the living animal. We now observed in vivo, when blocking Na^{+} channels from the inside with QX-314, slow spikes that had amplitudes and kinetics that were similar to the Ca^{2+} spikes reported previously in vitro. The slow spikes were driven by excitatory glutamatergic transmission, with an essential role of NMDA receptors. The strong attenuation of the slow spikes by D-890 points to a dominating role of voltage-gated Ca^{2+} channels for the slow depolarization. As D-890 is a broad-band Ca^{2+} channel antagonist, at least when applied at the high concentrations used here (Kovalchuk et al., 2000), the precise nature of the Ca^{2+} channel(s) involved in the generation of slow spikes are unclear. It is possible that R-type channels, as suggested by in vitro rat brain slice experiments (Takahashi and Magee, 2009), play a prominent role for CSs.

Under our recording conditions, the proximal apical and the basal dendrites were constantly activated by afferent inputs, as indicated by the frequently occurring local Ca^{2+} hot spots (Figures 4 and S4). These observations, together with those made in a previous study (Kamondi et al., 1998a), may suggest an important role of Schaffer collaterals in CS generation. Thus, burst activity arriving from the CA3 region (Csicsvari et al., 2000) is possibly a major determinant of CSs in CA1. Because of current technical limitations, calcium imaging of the activity in the apical tuft is not feasible and it remains therefore unclear whether, as observed in in vitro experiments, the coincident activity of Schaffer collaterals and perforant path contributes in a specific way to the spontaneous CS activity (Takahashi and Magee, 2009). Possibly, CSs are the result of the synaptic integration of spontaneous activity throughout the entire dendritic field, from basal to tuft dendrites. At time points of particularly frequent afferent excitatory activity, the dendritic depolarization could reach levels at which the Mg^{2+} block of dendritic NMDA receptor channels (Mayer et al., 1984) would become ineffective, leading to regenerative dendritic responses (Schiller et al., 2000). Such a mechanism could explain the pronounced voltage dependence of the CS frequency.

Finally, in contrast to previous observations that were made in basal dendrites of CA1 neurons in vitro (Ariav et al., 2003), the new dendritic Ca^{2+} spikes in vivo were not restricted individual dendrites but were true multidendrite events (Figures 4 and S4). The reason for the different findings most likely relates to the different modes of activation in the two different experimental conditions. While the local activation in slices, either through an extracellular stimulation pipette or local glutamate uncaging (Ariav et al., 2003), favors the activation of particular dendrites, the high level of afferent activity in vivo produces more global activation in wide dendrite-somatic fields (Figures 4H and 4I; Figure S4). Despite these differences, both the in vitro and in vivo recordings stress the strong role of NMDA receptors in CA1 pyramidal neurons for input-output transformations. The multidendrite Ca^{2+} spikes may be particularly relevant for activity-dependent synaptic plasticity, especially long-term potentiation (Grover et al., 2009; Harris et al., 2001; Magee and Johnston, 1997; Pike et al., 1999; Thomas et al., 1998). They may define "windows of opportunity" during which spine Ca^{2+} entry through NMDA receptor channels adds up with Ca^{2+} entry through voltage-gated Ca^{2+} channels, producing locally a supralinear Ca^{2+} signal. In this way, NMDA receptor-dependent

multidendrite Ca^{2+} spikes may promote the induction of plastic changes at simultaneously active weak synaptic inputs with a high reliability and efficiency.

EXPERIMENTAL PROCEDURES

Surgery

All experimental procedures were performed in accordance with institutional animal welfare guidelines and were approved by the state government of Bavaria, Germany. C57BL/6 mice (postnatal days 28–65, n = 27) were prepared for in vivo two-photon Ca^{2+} imaging and whole-cell patch-clamp recordings under isoflurane anesthesia. Surgery was carried out as described previously (Jia et al., 2010). To obtain access to the hippocampus, we carefully removed cortical tissue covering the CA1 region (Busche et al., 2012; Dombeck et al., 2010; Mizrahi et al., 2004).

In Vivo Electrophysiology

Targeted whole-cell patch-clamp recordings of CA1 pyramidal neurons were established by "shadow patching" (Kitamura et al., 2008). Neurons were dialyzed with an intracellular solution containing the fluorescent Ca^{2+} indicator Oregon green BAPTA-1 (OGB-1; 100–150 μm) and Alexa 594 (25–50 μM). In some recordings, biocytin (0.2%) or pharmacological agents (MK-801 1 mM; QX-314 1–3 mM; D-890 1–5 mM) were added to the intracellular solution. Whole-cell recordings were targeted to excitatory pyramidal neurons in the CA1 region of the hippocampus, based on the following criteria: (1) stereotaxic coordinates (Paxinos and Franklin, 2001), (2) cell body located within the stratum pyramidale, and (3) presence of apical and basal spiny dendrites that extended from the conical soma (Megías et al., 2001).

High-Speed Two-Photon Ca^{2+} Imaging

Dendrites that were located in the same focal plane were imaged at acquisition rates of 40–80 full frames per second through the use of a resonant galvo scanner-based two-photon imaging system (Varga et al., 2011). Ca^{2+} imaging was started approximately 10–15 min after establishing the whole-cell configuration, to allow the diffusion of the Ca^{2+} dye and/or of pharmacological agents into the dendrites. At this time point, the dendrites of the CA1 pyramidal neurons were well labeled by OGB-1 and Alexa 594. Somatic membrane potential changes and Ca^{2+} signals were recorded simultaneously. In general, basal dendrites and proximal apical dendrites were accessible to two-photon Ca^{2+} imaging (up to about 150 μm below the cell somata; see e.g., Figure S4C).

SUPPLEMENTAL INFORMATION

Supplemental Information includes Supplemental Experimental Procedures and four figures and can be found with this article online at http://dx.doi.org/10.1016/j.neuron.2014.01.014.

ACKNOWLEDGMENTS

We thank Christine Karrer for excellent technical assistance and Dr. Hongbo Jia for help with data analysis. This work was supported by an Advanced ERC grant to A.K., the EU FP7 program (Project Corticonic), and the Deutsche Forschungsgemeinschaft (IRTG 1373 and SFB870).

Accepted: December 24, 2013
Published: February 20, 2014

REFERENCES

Abraham, W.C., and Kairiss, E.W. (1988). Effects of the NMDA antagonist 2AP5 on complex spike discharge by hippocampal pyramidal cells. Neurosci. Lett. *89*, 36–42.

Ariav, G., Polsky, A., and Schiller, J. (2003). Submillisecond precision of the input-output transformation function mediated by fast sodium dendritic spikes in basal dendrites of CA1 pyramidal neurons. J. Neurosci. *23*, 7750–7758.

Azouz, R., Jensen, M.S., and Yaari, Y. (1996). Ionic basis of spike after-depolarization and burst generation in adult rat hippocampal CA1 pyramidal cells. J. Physiol. *492*, 211–223.

Benardo, L.S., Masukawa, L.M., and Prince, D.A. (1982). Electrophysiology of isolated hippocampal pyramidal dendrites. J. Neurosci. *2*, 1614–1622.

Busche, M.A., Chen, X., Henning, H.A., Reichwald, J., Staufenbiel, M., Sakmann, B., and Konnerth, A. (2012). Critical role of soluble amyloid-β for early hippocampal hyperactivity in a mouse model of Alzheimer's disease. Proc. Natl. Acad. Sci. USA *109*, 8740–8745.

Buzsáki, G., Penttonen, M., Nádasdy, Z., and Bragin, A. (1996). Pattern and inhibition-dependent invasion of pyramidal cell dendrites by fast spikes in the hippocampus in vivo. Proc. Natl. Acad. Sci. USA *93*, 9921–9925.

Chen, X., Leischner, U., Rochefort, N.L., Nelken, I., and Konnerth, A. (2011). Functional mapping of single spines in cortical neurons in vivo. Nature *475*, 501–505.

Conti, R., and Lisman, J. (2002). A large sustained Ca2+ elevation occurs in unstimulated spines during the LTP pairing protocol but does not change synaptic strength. Hippocampus *12*, 667–679.

Csicsvari, J., Hirase, H., Mamiya, A., and Buzsáki, G. (2000). Ensemble patterns of hippocampal CA3-CA1 neurons during sharp wave-associated population events. Neuron *28*, 585–594.

Dombeck, D.A., Harvey, C.D., Tian, L., Looger, L.L., and Tank, D.W. (2010). Functional imaging of hippocampal place cells at cellular resolution during virtual navigation. Nat. Neurosci. *13*, 1433–1440.

Epsztein, J., Brecht, M., and Lee, A.K. (2011). Intracellular determinants of hippocampal CA1 place and silent cell activity in a novel environment. Neuron *70*, 109–120.

Fujita, Y. (1975). Two types of depolarizing after-potentials in hippocampal pyramidal cells of rabbits. Brain Res. *94*, 435–446.

Golding, N.L., Jung, H.Y., Mickus, T., and Spruston, N. (1999). Dendritic calcium spike initiation and repolarization are controlled by distinct potassium channel subtypes in CA1 pyramidal neurons. J. Neurosci. *19*, 8789–8798.

Graves, A.R., Moore, S.J., Bloss, E.B., Mensh, B.D., Kath, W.L., and Spruston, N. (2012). Hippocampal pyramidal neurons comprise two distinct cell types that are countermodulated by metabotropic receptors. Neuron *76*, 776–789.

Grover, L.M., Kim, E., Cooke, J.D., and Holmes, W.R. (2009). LTP in hippocampal area CA1 is induced by burst stimulation over a broad frequency range centered around delta. Learn. Mem. *16*, 69–81.

Hahn, T.T., Sakmann, B., and Mehta, M.R. (2007). Differential responses of hippocampal subfields to cortical up-down states. Proc. Natl. Acad. Sci. USA *104*, 5169–5174.

Harris, K.D., Hirase, H., Leinekugel, X., Henze, D.A., and Buzsáki, G. (2001). Temporal interaction between single spikes and complex spike bursts in hippocampal pyramidal cells. Neuron *32*, 141–149.

Harris, K.D., Henze, D.A., Hirase, H., Leinekugel, X., Dragoi, G., Czurkó, A., and Buzsáki, G. (2002). Spike train dynamics predicts theta-related phase precession in hippocampal pyramidal cells. Nature *417*, 738–741.

Harvey, C.D., Collman, F., Dombeck, D.A., and Tank, D.W. (2009). Intracellular dynamics of hippocampal place cells during virtual navigation. Nature *461*, 941–946.

Izhikevich, E.M., Desai, N.S., Walcott, E.C., and Hoppensteadt, F.C. (2003). Bursts as a unit of neural information: selective communication via resonance. Trends Neurosci. *26*, 161–167.

Jarsky, T., Mady, R., Kennedy, B., and Spruston, N. (2008). Distribution of bursting neurons in the CA1 region and the subiculum of the rat hippocampus. J. Comp. Neurol. *506*, 535–547.

Jensen, M.S., Azouz, R., and Yaari, Y. (1994). Variant firing patterns in rat hippocampal pyramidal cells modulated by extracellular potassium. J. Neurophysiol. *71*, 831–839.

Jia, H., Rochefort, N.L., Chen, X., and Konnerth, A. (2010). Dendritic organization of sensory input to cortical neurons in vivo. Nature *464*, 1307–1312.

Kamondi, A., Acsády, L., and Buzsáki, G. (1998a). Dendritic spikes are enhanced by cooperative network activity in the intact hippocampus. J. Neurosci. *18*, 3919–3928.

Kamondi, A., Acsády, L., Wang, X.J., and Buzsáki, G. (1998b). Theta oscillations in somata and dendrites of hippocampal pyramidal cells in vivo: activity-dependent phase-precession of action potentials. Hippocampus *8*, 244–261.

Kandel, E.R., and Spencer, W.A. (1961). Electrophysiology of hippocampal neurons. II. After-potentials and repetitive firing. J. Neurophysiol. *24*, 243–259.

Kepecs, A., Wang, X.J., and Lisman, J. (2002). Bursting neurons signal input slope. J. Neurosci. *22*, 9053–9062.

Kitamura, K., Judkewitz, B., Kano, M., Denk, W., and Häusser, M. (2008). Targeted patch-clamp recordings and single-cell electroporation of unlabeled neurons in vivo. Nat. Methods *5*, 61–67.

Kovalchuk, Y., Eilers, J., Lisman, J., and Konnerth, A. (2000). NMDA receptor-mediated subthreshold Ca(2+) signals in spines of hippocampal neurons. J. Neurosci. *20*, 1791–1799.

Kuga, N., Sasaki, T., Takahara, Y., Matsuki, N., and Ikegaya, Y. (2011). Large-scale calcium waves traveling through astrocytic networks in vivo. J. Neurosci. *31*, 2607–2614.

Lisman, J.E. (1997). Bursts as a unit of neural information: making unreliable synapses reliable. Trends Neurosci. *20*, 38–43.

Magee, J.C., and Carruth, M. (1999). Dendritic voltage-gated ion channels regulate the action potential firing mode of hippocampal CA1 pyramidal neurons. J. Neurophysiol. *82*, 1895–1901.

Magee, J.C., and Johnston, D. (1997). A synaptically controlled, associative signal for Hebbian plasticity in hippocampal neurons. Science *275*, 209–213.

Mayer, M.L., Westbrook, G.L., and Guthrie, P.B. (1984). Voltage-dependent block by Mg^{2+} of NMDA responses in spinal cord neurones. Nature *309*, 261–263.

Megías, M., Emri, Z., Freund, T.F., and Gulyás, A.I. (2001). Total number and distribution of inhibitory and excitatory synapses on hippocampal CA1 pyramidal cells. Neuroscience *102*, 527–540.

Metz, A.E., Jarsky, T., Martina, M., and Spruston, N. (2005). R-type calcium channels contribute to afterdepolarization and bursting in hippocampal CA1 pyramidal neurons. J. Neurosci. *25*, 5763–5773.

Mizrahi, A., Crowley, J.C., Shtoyerman, E., and Katz, L.C. (2004). High-resolution in vivo imaging of hippocampal dendrites and spines. J. Neurosci. *24*, 3147–3151.

Mizuseki, K., and Buzsáki, G. (2013). Preconfigured, skewed distribution of firing rates in the hippocampus and entorhinal cortex. Cell Rep *4*, 1010–1021.

Mizuseki, K., Diba, K., Pastalkova, E., and Buzsáki, G. (2011). Hippocampal CA1 pyramidal cells form functionally distinct sublayers. Nat. Neurosci. *14*, 1174–1181.

Paulsen, O., and Sejnowski, T.J. (2000). Natural patterns of activity and long-term synaptic plasticity. Curr. Opin. Neurobiol. *10*, 172–179.

Paxinos, G., and Franklin, K.B.J. (2001). The Mouse Brain in Stereotaxic Coordinates. (San Diego: Academic Press).

Pike, F.G., Meredith, R.M., Olding, A.W., and Paulsen, O. (1999). Rapid report: postsynaptic bursting is essential for 'Hebbian' induction of associative long-term potentiation at excitatory synapses in rat hippocampus. J. Physiol. *518*, 571–576.

Ranck, J.B., Jr. (1973). Studies on single neurons in dorsal hippocampal formation and septum in unrestrained rats. I. Behavioral correlates and firing repertoires. Exp. Neurol. *41*, 461–531.

Rose, G., Pang, K., Palmer, M., and Freedman, R. (1984). Differential effects of phencyclidine upon hippocampal complex-spike and theta neurons. Neurosci. Lett. *45*, 141–146.

Sanabria, E.R., Su, H., and Yaari, Y. (2001). Initiation of network bursts by Ca2+-dependent intrinsic bursting in the rat pilocarpine model of temporal lobe epilepsy. J. Physiol. *532*, 205–216.

Schiller, J., Major, G., Koester, H.J., and Schiller, Y. (2000). NMDA spikes in basal dendrites of cortical pyramidal neurons. Nature *404*, 285–289.

Schwartzkroin, P.A., and Slawsky, M. (1977). Probable calcium spikes in hippocampal neurons. Brain Res. *135*, 157–161.

Strichartz, G.R. (1973). The inhibition of sodium currents in myelinated nerve by quaternary derivatives of lidocaine. J. Gen. Physiol. *62*, 37–57.

Suzuki, S.S., and Smith, G.K. (1985). Single-cell activity and synchronous bursting in the rat hippocampus during waking behavior and sleep. Exp. Neurol. *89*, 71–89.

Takahashi, H., and Magee, J.C. (2009). Pathway interactions and synaptic plasticity in the dendritic tuft regions of CA1 pyramidal neurons. Neuron *62*, 102–111.

Thomas, M.J., Watabe, A.M., Moody, T.D., Makhinson, M., and O'Dell, T.J. (1998). Postsynaptic complex spike bursting enables the induction of LTP by theta frequency synaptic stimulation. J. Neurosci. *18*, 7118–7126.

Varga, Z., Jia, H., Sakmann, B., and Konnerth, A. (2011). Dendritic coding of multiple sensory inputs in single cortical neurons in vivo. Proc. Natl. Acad. Sci. USA *108*, 15420–15425.

Wong, R.K., Prince, D.A., and Basbaum, A.I. (1979). Intradendritic recordings from hippocampal neurons. Proc. Natl. Acad. Sci. USA *76*, 986–990.

Xu, W., Morishita, W., Buckmaster, P.S., Pang, Z.P., Malenka, R.C., and Südhof, T.C. (2012). Distinct neuronal coding schemes in memory revealed by selective erasure of fast synchronous synaptic transmission. Neuron *73*, 990–1001.